PHYSICAL REVIEW B VOLUME 4, NUMBER 8 15 OCTOBER 1971

Energy Band Structure of Lithium Fluoride Crystals by the Method of Tight Binding

Roy C. Chaney
University of Texas at Dallas, Dallas, Texas 75230

and

Earl E. Lafon*
Department of Physics, Oklahoma State University, Stillwater, Oklahoma 74074

and

Chun C. Lin
Department of Physics, University of Wisconsin, Madison, Wisconsin 53706
(Received 14 June 1971)

The method of tight binding has been applied to calculate the energy band structure of the lithium fluoride crystal. As initial approximations to the ultimate self-consistent-field (SCF) calculations, two different overlapping atomic potentials were employed, one formed by a superposition of the potential of the neutral Li and F atoms, and the other by that of Li^+ and F^-. The resulting energy band gaps for these two potentials were 15.2 and 14.2 eV, respectively. A minimal set of the ten Bloch sums of the SCF wave functions of the $1s$, $2s$, and $2p$ states of the free Li and F atoms, a set of 30 contracted-Gaussian Bloch sums, and a set of 50 single-Gaussian Bloch sums have been used as the basis functions, and our calculations show that the minimal set is quite adequate for computing the energies of the valence band and the lowest conduction band. A computational procedure for incorporating the Hartree-Fock-Slater SCF scheme into the method of tight binding has been formulated and applied to carry out the energy band calculations of LiF to self-consistency. The SCF band structure gives an energy band gap of 10.9 eV in comparison with the experimental value of 13.6 eV. Our calculations place the top of the valence band 12.3 eV below the vacuum level, and the Li $1s$ core states 57 eV below the bottom of the conduction band, which may be compared with the observed onset of photoemission at 12 eV and photoabsorption structure at 60 eV.

I. INTRODUCTION

In a few recent papers[1-3] it was shown that the method of tight binding can be applied to calculate energy band structure of the alkali metals and group-IV crystals to a high degree of accuracy. The introduction of the Gaussian-type atomic orbitals to this method has enabled us to express all the matrix elements of the one-electron crystal Hamiltonian in analytic form, and has greatly reduced the computational work required to obtain the energy bands. It has also been pointed out that, for the alkali metals, the use of linear combination of atomic orbitals (LCAO) automatically generates conduction-band wave functions at the Γ point which exhibit the constant electron-density behavior of a free particle, and hence the validity of the method of tight binding is not limited to the "tightly bound" electrons. The term "method of LCAO" is indeed a more descriptive title[4] than the "method of tight binding," although we will continue to use these two names in an interchangeable way.

It is natural to extend the application of the method of tight binding to the alkali halide crystals. In view of its success in the cases of lithium, sodium, diamond, and silicon, this method may be expected to give very accurate band structure for LiF. The electrons in the valence band of the alkali halide crystals are, to a considerable extent, "bound" to their parent ions, and thus the method of tight binding should be particularly useful for analyzing the electron distribution in the crystals in terms of the charge distribution of the constituent ions.

In many works on energy band calculations, it is customary to approximate the crystal potential as the sum of the potential of the individual free atoms situated at the appropriate sites of the crystal lattice—sometimes called the overlapping-atomic-potential (OAP) model.[5] This approximation proves to be a good one for element crystals, but in the case of noncovalent binary-compound crystals, the validity of this simple OAP model may be questionable. Thus we shall adopt this OAP model only to obtain an initial approximation to the self-consistent-field (SCF) band structure (Sec. II), and then carry out the solution to self-consistency by iteration in Sec. III. A discussion of the crystal charge distribution and comparison of the calculated band structure with the experimental observations will also be given. In this paper, our primary interests are focused on the valence band and the

lowest conduction band. The higher conduction bands, particularly their relations to the atomic d states of the constituent ions, will be investigated in a subsequent work.

II. OVERLAPPING ATOMIC POTENTIAL

Under the OAP model we approximate the charge density of the crystal by a superposition of the spherically averaged charge densities of the individual fluorine and lithium units (ζ_1 and ζ_2, respectively) in the lattice, i.e.,

$$\rho_{\rm cry}(\vec{r}) = \sum_\nu [\zeta_1(|\vec{r} - \vec{R}_\nu|) + \zeta_2(|\vec{r} - \vec{R}_\nu - \vec{T}|)], \quad (1)$$

where $\vec{R}_\nu$ refers to the position vectors of the fluorine atoms and $\vec{T}$ is a vector drawn from a fluorine atom to one of its nearest-neighbor lithium atoms. To calculate $\rho_{\rm cry}$, one can take ζ_1 and ζ_2 either as the charge density of the neutral fluorine (spherically averaged) and of the neutral lithium atom, respectively, or as that of F^- and of Li^+, respectively. The choice between such a "neutral-atom model" and an "ionic model" is somewhat arbitrary at this point, in view of the lack of a quantitative knowledge of the electron distribution in the crystal. Since the OAP is used here only as a starting point for the SCF calculation, we can adopt either one of the two above-mentioned models as the initial approximation. Nevertheless, for the purpose of comparison we have examined both the neutral-atom and ionic models, and found only a rather small difference between the band structures resulting from these two models.

The crystal potential is composed of contributions from Coulomb interaction and from exchange as

$$V_{\rm cry}(\vec{r}) = V_{\rm cry}{}^C(\vec{r}) + V_{\rm cry}{}^E(\vec{r}). \quad (2)$$

The former can be obtained from ζ_1 and ζ_2 in the standard way,[6] and the latter is replaced by the Slater approximation $-\frac{3}{2}(3\rho_{\rm cry}/\pi)^{1/3}$. Although it is customary to further approximate the Slater exchange term as a superposition of the individual atomic terms $-\frac{3}{2}(3\rho_{\rm atom}/\pi)^{1/3}$, this step will not be taken in the present work. To facilitate the numerical computation, we curve fit the Slater exchange potential to a superposition of atomlike functions centered about each of the lattice sites as

$$V_{\rm cry}^E(\vec{r}) = -\tfrac{3}{2}(3\rho_{\rm cry}/\pi)^{1/3} = \sum_\nu [\eta_1(|\vec{r} - \vec{R}_\nu|) + \eta_2(|\vec{r} - \vec{R}_\nu - \vec{T}|)], \quad (3)$$

where the η's are chosen to have the form

$$\eta_i(r) = e^{-\kappa_i r} \sum_{j=0}^{4} c_{ij} r^j, \quad (4)$$

with κ_i and c_{ij} being the adjustable parameters for curve fitting. If we place the origin of the coordinate system at one of the atomic sites, e.g., a fluorine atom, then the crystal potential, on account of its inversion symmetry, can be expanded as a cosine series,

$$V_{\rm cry}(\vec{r}) = \sum_\nu V_{\rm cry}(\vec{K}_\nu)\cos(\vec{K}_\nu \cdot \vec{r}), \quad (5)$$

where

$$V_{\rm cry}(\vec{K}_\nu) = 4\pi K_\nu^{-2}\Omega^{-1}\left(-Z_F + \int_0^\infty [4\pi K_\nu^{-1}\zeta_1(r) + K_\nu \eta_1(r)]\, r \sin(K_\nu r)\, dr\right) + 4\pi K_\nu^{-2}\Omega^{-1}\cos(\vec{K}_\nu \cdot \vec{T}) \times\left(-Z_{\rm Li} + \int_0^\infty [4\pi K_\nu^{-1}\zeta_2(r) + K_\nu \eta_2(r)] r \sin(K_\nu r)\, dr\right). \quad (6)$$

Here $Z_{\rm F}$ and $Z_{\rm Li}$ are the atomic numbers of fluorine and lithium, respectively. For computating the electron densities ζ_1 and ζ_2, we used the SCF wave functions of Li, F, and Li^+ tabulated by Clementi,[7] and those of F^- given by Clementi and McLean.[8] We have compared the wave functions of Clementi and McLean for a free F^- ion with those of an F^- ion in the ionic lattice of LiF,[9] and found rather little difference between them. Figure 1 shows the crystal charge densitites along the [100] line of the lattice calculated by Eq. (1). The two sets of charge densities calculated by using the neutral-atom model and by using the ionic model differ from each other by no more than a few percent throughout the entire range of Fig. 1, and are represented by the same curve (solid curve), as their differences are too small to be displayed clearly in this figure. The close resemblance between these two sets of charge density is quite remarkable considering the seemingly drastic difference in viewpoint between the ionic and neutral-atom descriptions. The reason is that in the neutral-atom picture the 2s wave function of Li overlaps strongly with the F atoms, whereas the fluorine 2s and 2p orbitals are less diffuse and overlap to a much less extent with the neighboring atoms. This is equivalent to a transfer of charge from the Li to the F atoms, resulting in ionic properties even under a neutral-atom model.[10]

A natural choice of the basis functions is the ten Bloch sums of the 1s, 2s, 2p_x, 2p_y, 2p_z SCF wave functions of the neutral Li and F atoms, e.g.,

$$b_{1s}^{\rm F}(\vec{k}, \vec{r}) = \sum_\nu e^{i\vec{k}\cdot\vec{R}_\nu}\phi_{1s}^{\rm F}(\vec{r} - \vec{R}_\nu), \quad b_{1s}^{\rm Li}(\vec{k}, \vec{r}) = \sum_\nu e^{i\vec{k}\cdot(\vec{R}+\vec{T})}\phi_{1s}^{\rm Li}(\vec{r} - \vec{R}_\nu - \vec{T}). \quad (7)$$

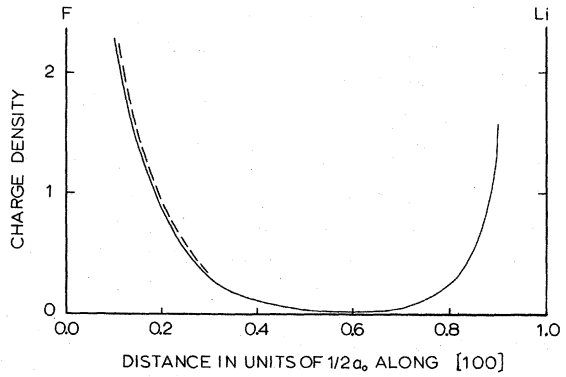

FIG. 1. Electronic charge density of the LiF crystal along the [100] direction between a Li and a F site. The charge densities calculated by the neutral-atom OAP and by the ionic OAP are nearly the same, and are represented by the solid curve. The dashed curve gives the charge densities obtained from the SCF crystal wave functions. At distances larger than 0.3 units of the abscissa scale, the SCF and OAP charge densities are too close to be distinguished in the graph.

The Gaussian-type SCF atomic wave functions have been given by Huzinaga[11] and by Chaney *et al.*[2] To illustrate the overlap of the valence orbitals of Li with the F sites, we have plotted the Bloch sums b_{2s}^{Li}, b_{2s}^{F}, and b_{2px}^{F} for $\vec{k}=0$ along the [100] line of the crystal in Fig. 2. Analogous to the idea of charge transfer from the Li to the F atoms, one observes that the Li Bloch sum gravitates toward the F atoms, whereas the two F Bloch sums are more localized around their parent sites.

To obtain the band structure we set up the 10×10 energy matrix of the crystal Hamiltonian based on the neutral-atom model. The procedure for calculating the matrix elements of the overlap, kinetic-energy, and potential-energy terms has been described in our previous papers[1,2] and will not be repeated here. With this ten-function basis set one should be able to get quite accurate energies for the core states, the valence band, and the lowest conduction band. However, the three highest roots of the 10×10 secular equations which correspond to the higher conduction band (Γ_{15}', X_1, X_5', L_2', L_3) are expected to be less accurate because of the limited size of the basis set. To provide more variational freedom, we have replaced the five Li atomic-orbital Bloch sums by the Bloch sums of the contracted Gaussians as was done in Eqs. (9) of Ref. 2. In a similar manner we form three sets of three-member contracted Gaussians for the s functions of F. There are five Gaussian exponents in the $2p$ atomic wave function of F; they are divided into two sets of two-member contraction (with the two highest exponents in one group and the two lowest in the other) plus the remaining one-member Gaussian. The energies calculated by this basis set of 30 contracted-Gaussian Bloch sums are shown in Table I.[12] For the valence band and the lowest conduction band, the lowering of the eigenvalues due to the use of contracted Gaussians over the SCF atomic orbitals are rather small, typically 0.005 a.u. On the other hand, the energy of the X_5' state of the higher conduction band decreased by 0.105 a.u. as one changed from the 10-basis set of Bloch sums of SCF atomic orbitals to the contracted-Gaussian Bloch sums. To further increase the number of basis functions, we have adopted a set of 50 single-Gaussian Bloch sums: nine $1s$-F and five $2p$-F Bloch sums with exponents listed in Ref. 11, eight $1s$-Li Bloch sums with exponents of Ref. 11 except the smallest one, and six $2p$-Li Bloch sums with exponents of Ref. 2 except the smallest one. The Bloch sums formed by the two omitted long-range Gaussian overlap very strongly with the corresponding Bloch sums of higher exponents already included, and therefore offer very little additional variational freedom. The energies derived from this 50-basis set are given in Table I. Except for the L_{3c}' point in the higher conduction band, the energies computed by means of the single-Gaussian set differ little from those by the contracted-Gaussian basis. The energy band gap obtained by this calculation is 15.2 eV compared with the experimental value of 13.6 eV reported by Roessler and Walker.[13]

We have changed the crystal potential into the one of the ionic model, and calculated the band structure using the ten-basis functions defined in Eqs. (7). The band gap now becomes 14.2 eV and the energies of some of the states of the valence band and the lowest conduction band (relative to the top of the valence band) are -0.0588, -0.0200, 0.693, -0.531, -0.0052, and 0.640 a.u. for X_{4v}', X_{5v}', X_{4c}',

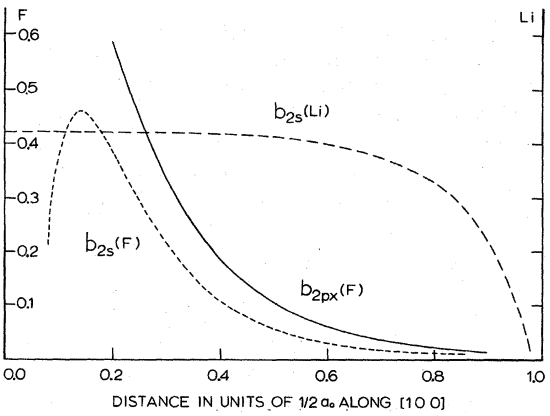

FIG. 2. Values of the Bloch sums formed by the atomic $2s$ state of Li (dashed curve), by the $2s$ state of F (dotted curve), and by the $2px$ state of F (solid curve), for $\vec{k}=0$ along the [100] line of the crystal between a Li and F site.

TABLE I. Energy bands of LiF calculated by using the neutral-atom model OAP with a 30-basis set (contracted Gaussians) and a 50-basis set (single Gaussians).

	Energies (in a.u.)	
	30×30	50×50
Γ_{15v}	−0.927	−0.928
X'_{4v}	−0.978	−0.979
X'_{5v}	−0.944	−0.945
L'_{2v}	−0.972	−0.972
L'_{3v}	−0.931	−0.932
Γ_{1c}	−0.368	−0.369
X'_{4c}	−0.200	−0.205
L_{1c}	−0.249	−0.269
Γ_{15c}	0.241	0.236
X_{1c}	−0.021	−0.029
X'_{5c}	0.067	0.050
L'_{2c}	−0.132	−0.132
L_{3c}	0.114	0.060

L'_{2v}, L'_{3v}, and L_{1c}, respectively.

III. SELF-CONSISTENT-FIELD CALCULATION

The OAP potential is found to be far from self-consistent, and thus an iterative technique which is readily applicable to the tight-binding scheme must be developed. In this procedure the band structure is used to predict the electronic charge density of the crystal in the usual manner, i.e.,

$$\rho_{\rm cry}(\vec{\mathbf{r}}) = -2N\Omega(2\pi)^{-3}\int_{\rm B.Z.}\sum_{ni} g_n(\vec{\mathbf{k}})\,|\psi_{ni}(\vec{\mathbf{k}},\vec{\mathbf{r}})|^2\,d\vec{\mathbf{k}}\,, \tag{8}$$

where N represents, symbolically, the number of unit cells in the crystal, Ω is the volume of the primitive unit cell, n labels the band index and i the degeneracies (excluding spin) within the band for each point $\vec{\mathbf{k}}$ in the Brillouin zone, and $g_n(\vec{\mathbf{k}})$ is unity or zero depending on whether the band is occupied or not. This integral is evaluated by numerical quadrature, and the summation over discrete points in the Brillouin zone must be performed in such a manner that the invariance of the total charge density under all operations of the space group is preserved. The resultant $\rho_{\rm cry}(\vec{\mathbf{r}})$ is evaluated over a tabular mesh of points which cover a fundamental wedge of the unit cell with volume $\Omega/48$. The values of $\rho_{\rm cry}(\vec{\mathbf{r}})$ at equivalent points outside this fundamental wedge can be directly obtained from one or more of the 48 operations of the site group. This tabular expression for charge density is then curve fitted to the analytic form

$$\rho_{\rm cry}(\vec{\mathbf{r}}) = \sum_\nu [\rho_1(\vec{\mathbf{r}}-\vec{\mathbf{R}}_\nu)+\rho_2(\vec{\mathbf{r}}-\vec{\mathbf{R}}_\nu-\vec{\mathbf{T}})]\,, \tag{9}$$

where

$$\rho_i(\vec{\mathbf{r}}) = \sum_{lm} a_{lm}^{(i)}(r)\,Y_{lm}(\theta\phi), \quad i=1,2\,. \tag{10}$$

One may notice some similarity between Eqs. (9) and (1). The functions ζ in Eq. (1) refer to the charge densities (spherically averaged) of the constituent atoms or ions of the crystal, whereas ρ_1 and ρ_2 are, in general, angular-dependent functions and are designed to fit the crystal charge density, which we obtained from Eq. (8), in accordance with the form of Eq. (9). The requirement that $\rho_{\rm cry}(\vec{\mathbf{r}})$ be invariant under all the operations of the space group will be satisfied if $\rho_1(\vec{\mathbf{r}})$ and $\rho_2(\vec{\mathbf{r}})$ are required to be invariant under their respective site groups. This restriction leads to the $l=1$, 2, and 3 terms in Eq. (10) being forbidden by symmetry, and the first two nonvanishing terms in this expansion correspond to $l=0$ and $l=4$. Direct evaluation of the $l=4$ term in LiF shows this contribution to be extremely small; thus the expansion terms with $l\geq4$ are neglected for this material. The neglection of the nonzero values of l is not always justified; for example, in the case of diamond where strong tetrahedral bonds are formed, it is found necessary to include both the $l=0$ and $l=3$ terms from Eq. (10) in order to obtain an adequate representation of the self-consistent charge density.[14] It should also be recognized that the inclusion of only $l=0$ in Eq. (10) does not mean that the charge environment around each atom is taken to be spherical, since $\rho_{\rm cry}$ is written as a superposition of ρ_1 and ρ_2, and the overlap of the contributions of the neighboring atoms automatically produces a nonspherical charge distribution around each atomic site.

From Eqs. (9) and (10), a Fourier expansion of the electronic charge density may be performed as

$$\rho_{\rm cry}(\vec{\mathbf{r}}) = \sum_\nu \rho_{\rm cry}(\vec{\mathbf{K}}_\nu)\cos(\vec{\mathbf{K}}_\nu\cdot\vec{\mathbf{r}})\,, \tag{11}$$

$$\rho_{\rm cry}(\vec{\mathbf{K}}_\nu) = \rho_1(\vec{\mathbf{K}}_\nu)+e^{-i\vec{\mathbf{K}}_\nu\cdot\vec{\mathbf{T}}}\,\rho_2(\vec{\mathbf{K}}_\nu)\,, \tag{12}$$

$$\rho_k(\vec{\mathbf{K}}_\nu) = \Omega^{-1}\int\rho_k(\vec{\mathbf{r}})\,e^{-i\vec{\mathbf{K}}_\nu\cdot\vec{\mathbf{r}}}\,d\tau$$

$$= \frac{4\pi}{\Omega}\sum_{lm}(-i)^l\,Y_{lm}(\hat{K}_\nu)\int_0^\infty r^2 a_{lm}^{(k)}\,j_l(K_\nu r)\,dr\,, \tag{13}$$

where j_l is the spherical Bessel function. If the $a_{lm}^{(j)}(r)$ are chosen to be of the form

$$a_{lm}^{(j)}(r) = \sum_n \alpha_{lmn,j}\,r^{\beta_{n,j}}\,e^{-\gamma_{n,j}r}\,, \tag{14}$$

Eq. (13) reduces to

$$\rho_j(\vec{\mathbf{K}}_\nu) = \frac{4\pi}{\Omega}\sum_{lmn}(-i)^l\alpha_{lmn,j}\,Y_{lm}(\hat{K}_\nu)$$

$$\times \chi(\beta_{n,j}+2,\, l,\, \gamma_{n,j};\, K_\nu)\,, \qquad (15)$$

where

$$\chi(\mu, n, p; a) \equiv \int_0^\infty r^\mu j_n(ar)\, e^{-pr}\, dr$$

$$= 2^{-n} a^{-(n+1)} (p^2+a^2)^{(n-\mu)/2}\, \Gamma(\mu+n+1)$$

$$\times \sum_l \frac{(-1)^l \Gamma(n+1)\Gamma(\mu+l-n)}{\Gamma(n-l+1)\Gamma(\mu+l+1) l!}$$

$$\times \sin\left((2l+\mu-n)\tan^{-1}\frac{a}{p}\right)\,. \qquad (16)$$

The above expression is valid for $p>0$, $\mu+n>-1$. When μ is equal to an integer less than or equal to n, certain individual terms in the above sum diverge. However, a limiting procedure can be adopted to cancel the divergent terms. Once the Fourier coefficients of the electronic charge density have been computed, the Coulomb contribution to the one-electron potential is easily obtained via Poisson's equation.

In a similar manner, the exchange contribution to the crystal potential can be calculated by curve fitting the exchange term as

$$-\tfrac{3}{2}\left[3\rho_{\rm cry}(\vec{r})/\pi\right]^{1/3} = \sum_\nu \left[f_1(\vec{r}-\vec{R}_\nu) + f_2(\vec{r}-\vec{R}_\nu-\vec{T})\right]\,. \qquad (17)$$

Once this is done, the Fourier coefficients $V^E_{\rm cry}(\vec{K}_\nu)$ of the exchange potential are readily obtainable. The necessary Fourier coefficients of the crystal potential $V_{\rm cry}(\vec{K}_\nu)$ are then given by

$$V_{\rm cry}(\vec{K}_\nu) = -(4\pi/\Omega K_\nu^2)\left[Z_{\rm F} + Z_{\rm Li} e^{-i\vec{K}_\nu\cdot\vec{T}} - \rho_1(\vec{K}_\nu)\right.$$

$$\left. - \rho_2(\vec{K}_\nu) e^{-i\vec{K}_\nu\cdot\vec{T}}\right] + V^E_{\rm cry}(\vec{K}_\nu)\,. \qquad (18)$$

This new potential which is constructed from the band structure is then used in an iterative procedure until self-consistency is achieved. In order to speed up the convergence to self-consistency, the potential used in each iteration is constructed by averaging the predicted potential with those of previous iterations.

In this SCF calculation we first use as the basis functions the ten Bloch sums corresponding to the $1s$, $2s$, $2p$ functions of the neutral Li and F atoms and a three-point integration scheme over the Brillouin zone using points Γ, X, L, with a relative weighting of 1:3:4. The results for the valence band and the lowest conduction band are presented in column A of Table II. Here we have set the energy of the top of the valence band as zero. The calculations of the Fourier component for $\vec{K}_\nu=0$, $V_{\rm cry}(0)$ of the crystal potential and the energy of the valence band relative to the vacuum level will be deferred to Sec. IV. We then used the set of 50 basis functions of single-Gaussian Bloch sums described in Sec. II along with the same SCF crystal potential used in column A to recalculate the band structure. The resulting energies are shown in column B of Table II. We have adopted the same "zero" reference point in the energy scale for columns A and B. It is seen that an augmentation of the basis set has only very small effects on the energies of the valence band and of the lowest conduction band, and the ten-member set appears to be quite adequate for our purpose. To improve the k-point integration, we increase the number of quadrature points from three to five by including points midway along the Δ and λ lines of the Brillouin zone, and the SCF iteration is repeated by using the ten-member basis set. The last column of Table II gives the energies of this five-point quadrature calculation. Again we have taken the energy of the Γ_{15} state as the zero-energy point; this zero reference is different from that used in columns A and B. The close resemblance between the entries in columns A and C indicates good convergence of the valence band and the lowest conduction band with respect to the integration over the Brillouin zone.

Figure 3 shows the SCF band structure obtained by the ten-member basis set and five-point quadrature integration over the k space. The energy band gap is 10.9 eV, which is considerably lower than the values of 15.2 and 14.2 eV obtained in Sec. II, indicating the inadequacy of the OAP model for the case of LiF. As illustrated in the preceding paragraph, in spite of the very limited number of basis functions employed in the calculations, the energy bands shown in Fig. 3 are quite accurate within the

TABLE II. SCF energy bands of LiF calculated by a ten-basis set and three-point quadrature (column A), by a 50-basis set with the same crystal potential as used in A (column B), by a ten-basis set and five-point quadrature (column C).

	Energies (in a.u.)[a]		
	A	B	C
Γ_{15v}	0.000	−0.003	0.000
X'_{4v}	−0.083	−0.086	−0.087
X'_{5v}	−0.028	−0.031	−0.029
L'_{2v}	−0.073	−0.075	−0.077
L'_{3v}	−0.007	−0.009	−0.007
Γ_{1c}	0.408	0.402	0.395
X'_{4c}	0.604	0.597	0.594
L_{1c}	0.522	0.488	0.508

[a]The energies listed in columns A and B refer to the same zero reference point, which differs from that used for column C.

limit of the Hartree-Fock-Slater model. For the higher conduction bands a larger basis set must be used. Furthermore, the Bloch sums formed by the d-type orbitals may also play an important role for some of these higher states. Nevertheless, augmentation of the basis set over the minimal ten functions has very little effect on the wave functions of the core states and of the valence band, and thus would not appreciably alter the SCF crystal potential. To a very good approximation, one can therefore obtain the higher conduction bands by using the same crystal potential which produces the energy bands in Fig. 3. Investigations of the higher bands, however, are beyond the scope of this paper, and will be pursued more fully in a subsequent work.

The energy bands of LiF have been calculated previously by Page and Hygh[15] and by Kunz, Miyakawa, and Oyama.[16] Neither of these two calculations is of the SCF type. Page and Hygh employed a muffin-tin crystal potential which includes nonspherical potential terms, and solved the one-electron problem by the method of augmented plane waves. They further adjusted the coefficient of the Slater exchange potential to fit the experimental band-gap data. In the work of Kunz, Miyakawa, and Oyama, the method of mixed basis was used in conjunction with an OAP-type potential; however, their scheme of construction of the crystal potential is quite different from ours. Our band structures show the same general trends as those of Page and Hygh,[17] but differ even qualitatively from the results of Kunz, Miyakawa, and Oyama. In view of vast difference in the method of approach and calculations between our work and the work of Refs. 15 and 16, no detailed comparison of these three sets of results will be made.

IV. DISCUSSION

The charge densities obtained from the SCF band structure are shown as the dotted curve in Fig. 1. In comparing the SCF with the OAP charge densities, we found the SCF values to be appreciably higher in the vicinity around each F site (up to a distance of about 30% of that to its nearest Li site). These regions constitute only a small fraction of the total volume of the crystal. Outside these regions, the charge densities computed by the SCF wave functions become slightly lower than the OAP counterparts, although the differences are too small to be displayed in Fig. 1. The shift of the electron clouds toward the F sites as suggested by the SCF results can be understood at least qualitatively from the contraction of electron charge distribution toward the nucleus of an F^- ion when it is surrounded by six positive charges as in the LiF crystals.

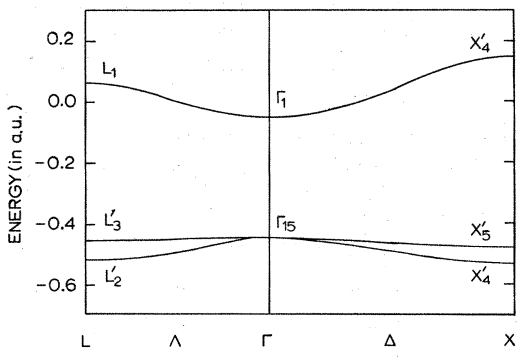

FIG. 3. Energy band structure of the LiF crystal calculated by the SCF tight-binding method using ten basis functions and a five-point quadrature for integration over the k space.

As may be expected of an ionic crystal, the charge density becomes very small in certain regions between the atomic sites. Furthermore, the "contraction" of the negative charge of F^- (due to the use of the SCF crystal wave functions) discussed in the preceding paragraph causes the charge clouds to segregate more than what would be anticipated from the simple ionic model. This is contrary to the case of a covalent crystal like diamond, in which the crystal wave functions give an enhancement of the charge density around the midpoint between two nearest-neighboring carbon atoms over the results of superposition of atomic charge distribution.[3] To investigate the charge distribution in the LiF crystal more quantitatively, we have calculated the amount of charge enclosed in spheres of different radii centered at a Li site. The results are shown in Fig. 4. We note that the curve shows a plateau at the region corresponding to two units of charge. This signifies that each Li nucleus is indeed surrounded by two electrons; thus the idea of regarding Li^+ as a constituent of the LiF crystal not only is qualitatively valid but also quantitatively reflects the actual charge distribution. One may also note that the plateau of the solid curve occurs at four-tenths of the distance to the nearest F site which, according to Fig. 1, is also the region of minimum charge density. For the purpose of comparison, the amounts of electronic charge of a single free Li^+ ion inside spheres of various radii have been computed and shown as dots in Fig. 4 along with the solid curve. We see no perceptible difference between the solid and the dotted curves up to the distance of 0.4 abscissa units, indicating that the charge distribution around the Li^+ in the crystal is essentially the same as that of a free Li^+ ion. Figure 4 also displays (the dashed curve) the electronic charges inside various spheres around a F site. At the plateau region of the solid curve, the dashed curve gives a charge of 9.5 units. The corresponding values of electronic charge for a

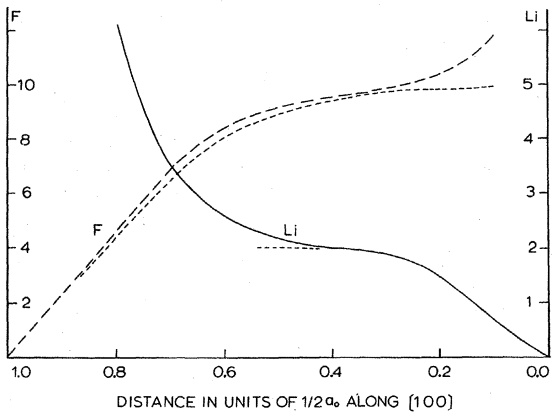

FIG. 4. Electronic charge distributions around a Li and a F site. The amounts of electronic charge of a LiF crystal enclosed in spheres of various radii around a Li site in the lattice are shown as the solid curve, and those around a F site as the dashed curve. The corresponding quantities of a free Li^+ ion and a F^- ion are given as the accompanying dotted curves. The ordinate scale for the Li curves is labeled in the right and that for the F curves in the left of the graph.

single free F^- ion are presented as the accompanying dotted curve. For the F^- ion in the LiF crystal, we do see a clear, though small, departure of the electron charge distribution from that of a free ion.

Our calculation gives an energy band gap of 10.9 eV as compared to the experimental value of 13.6 eV determined by Roessler and Walker.[13] As was shown in Sec. III, the value of the band gap changes very little as we augment the basis set from 10 to 50 Bloch sums. Furthermore, both the Γ_{15} and Γ_1 states involved in the band gap are not affected by the d orbitals. Thus the value of 10.9 eV should represent quite accurately the band gap of LiF which one would obtain under the Hartree-Fock-Slater scheme of the one-electron band model. We feel, therefore, that the discrepancy between the theoretical and measured band gap is due to the experimental uncertainties, or the limitation of the Hartree-Fock-Slater model, or both. Photoabsorption structure of LiF at 60 eV and above has been found in recent experiments.[18,19] They were attributed to transitions from the Li core states to the conduction-band states. Our calculations give the energy spacing between the Li 1s core and the bottom conduction band at the Γ point as 57 eV. Absorption bands in the energy regions of 15, 17, and 21 eV have also been reported.[13,20,21] It was suggested[15] that these bands may be associated with transitions at L and X, but no detailed identification has been given. While our calculated band structures indeed give the $L_3' - L_1$, $X_5' - X_4'$, and $L_3' - L_2'$ transitions in about the same energy ranges as the three absorption bands cited above, detailed comparison between theory and experiment concerning these three bands will not be attempted in view of the lack of certainty of the spectral identification.

With the SCF charge density it is possible to compute the Fourier component of the crystal potential corresponding to $\vec{K}_v = 0$, $V_{cry}(0)$, and thus locate the valence band relative to the vacuum level. The computation of $V_{cry}(0)$ is particularly facilitated by having the crystal charge density expressed in the form of Eq. (9). The Coulomb part of $V_{cry}(0)$ can then be obtained from $\rho_1(\vec{r})$ and $\rho_2(\vec{r})$, and the exchange part from $f_1(\vec{r})$ and $f_2(\vec{r})$ as defined in Eq. (17).[6,22] The value of $V_{cry}(0)$ depends quite sensitively on $\rho_1(\vec{r})$ and $\rho_2(\vec{r})$, and hence an extremely careful curve fitting of the SCF crystal charge density by Eq. (9) must be performed. This gives the vacuum level at 12.3 eV above the top of the valence band, which is consistent with the experimental photoemission data showing an onset at 12 eV for LiF.[23] If, instead of the SCF charge density, we use the OAP approximation to calculate $V_{cry}(0)$, we would obtain the energy of Γ_{15v} relative to the vacuum level as -24.9 and -17.4 eV for the neutral-atom and ionic models, respectively. Thus for the case of LiF, the energy bands relative to the vacuum level depend more sensitively on the detailed charge distribution than do the spacings between the bands.

---

*Work supported by Contract No. F33615-71-C-1395 issued by Aerospace Research Laboratory, Air Force Systems Command, U. S. Air Force, Wright-Patterson AFB, Ohio.

[1]E. E. Lafon and C. C. Lin, Phys. Rev. 152, 579 (1966).

[2]R. C. Chaney, T. K. Tung, C. C. Lin, and E. E. Lafon, J. Chem. Phys. 52, 361 (1970).

[3]R. C. Chaney, C. C. Lin, and E. E. Lafon, Phys. Rev. B 3, 459 (1971).

[4]J. C. Slater, *Quantum Theory of Molecules and Solids* (McGraw-Hill, New York, 1965), Vol. 2.

[5]F. Herman and S. Skillman, in *Proceedings of the International Conference on Semiconductor Physics, Prague*, 1960 (Academic, New York, 1961), p. 20; D. J. Stukel, R. N. Euwema, T. C. Collins, F. Herman, and R. L. Kortum, Phys. Rev. 179, 740 (1969).

[6]T. O. Woodruff, Solid State Phys. 4, 367 (1957).

[7]E. Clementi, IBM J. Res. Develop. 9, 2 (1965), and the supplement to this paper (unpublished).

[8]E. Clementi and A. D. McLean, Phys. Rev. 133, A419 (1964).

[9]K. Mansikka and F. Bystrand, J. Phys. Chem. Solids 27, 1073 (1966).

[10]The relation between the neutral-atom model and the ionic model has been pointed out by Slater. See Ref. 4, p. 111.

[11]S. Huzinaga, J. Chem. Phys. 42, 1243 (1965), Tables XI and XIII.

[12]The notations of the irreducible representations for

the groups X and L used here are given in J. Callaway, *Energy Band Theory* (Academic, New York, 1964), Chap. 1.

[13]D. M. Roessler and W. C. Walker, J. Phys. Chem. Solids 28, 1507 (1967).

[14]E. Lafon, MIT Solid State and Molecular Theory Group Quarterly Progress Report No. 69, 1968 (unpublished), p. 66.

[15]L. J. Page and E. H. Hygh, Phys. Rev. B 1, 3472 (1970).

[16]A. B. Kunz, T. Miyakawa, and S. Oyama, Phys. Status Solidi 34, 581 (1969).

[17]Our notations for the labels of the energy levels at the L point are different from those of Ref. 13. See Ref. 12.

[18]R. Haensel, C. Kunz, and B. Sonntag, Phys. Rev. Letters 20, 262 (1968).

[19]F. C. Brown, C. Gähwiller, A. B. Kunz, and N. O. Lipari, Phys. Rev. Letters 25, 927 (1970).

[20]A. Milgram and M. P. Gwens, Phys. Rev. 125, 1506 (1962).

[21]C. Gout and F. Pradel, J. Phys. Chem. Solids 29, 581 (1968).

[22]F. Herman, Phys. Rev. 93, 1214 (1954).

[23]S. W. Duckett and P. H. Metzger, Phys. Rev. 137, A953 (1965).

PHYSICAL REVIEW B VOLUME 4, NUMBER 8 15 OCTOBER 1971

Determination of Vacancy Jump Frequencies from Dielectric Loss Measurements on Ni^{++}-Doped NaCl Crystals

Krishan Lal and D. R. Pahwa
National Physical Laboratory, Hillside Road, New Delhi-12, India

(Received 21 January 1971)

Small divalent cation impurities such as Co, Mg, Mn, Ni, etc., in alkali halide crystals give two dielectric relaxation peaks, as they are associated with the nearest-neighbor (nn) and the next-nearest-neighbor (nnn) vacancies. NaCl: Ni^{++} crystals give peaks at frequencies (in Hz) of $(3.69\pm0.37)\times10^{11}e^{-0.62\pm0.06\ \mathrm{eV}/kT}$ and $(2.84\pm0.28)\times10^{11}e^{-(0.55\pm0.05\ \mathrm{eV})/kT}$. The jump frequencies ω_0 ($\omega_0=\omega_1+\omega_2$), ω_3, and ω_4 are expressed in terms of the positions of the two peaks and the ratio of the heights of the two peaks. ω_1, ω_2, ω_3, and ω_4 are the field-free jump frequencies of the cation vacancy defined by (i) ω_1, nn → nn; (ii) ω_2, nn → impurity; (iii) ω_3, nnn → nn; and (iv) ω_2, nn → nnn. At 80 °C, the values of jump frequencies ω_0, ω_3, and ω_4 were found to be $(1.54\pm0.17)\times10^4$, $(1.19\pm0.18)\times10^3$, and $(1.20\pm0.20)\times10^3$ Hz, respectively. It is seen that $\omega_0>\omega_3$, ω_4 and that ω_3 and ω_4 are almost equal in magnitude. From the latter fact it is concluded that the concentration of nn and nnn vacancies is almost equal. The relative values of ω_0, ω_3, and ω_4 are consistent with the earlier results of anelastic relaxation measurements.

I. INTRODUCTION

Divalent metallic impurities in alkali halide crystals form dipoles with oppositely charged vacancies.[1,2] These dipoles tend to orient along the externally applied electric field, giving rise to relaxational losses.[3] Several authors have observed dielectric-loss peaks due to such dipoles.[4-9]

For small impurity cations such as Co,[8,9] Mn,[10] and Mg,[7] two dielectric-loss peaks have been observed. Dreyfus[7] suggested that in such cases the cation vacancy can occupy both the nearest-neighbor (nn) and next-nearest-neighbor (nnn) positions relative to the impurity, and that $\tan\delta$ can be expressed as a sum of contributions from two Debye peaks. The exact expression for $\tan\delta$ is[7]

$$\tan\delta=\frac{16\pi a^2e^2N_ip}{3(2+\omega_4/\omega_3)\epsilon kT(\lambda_1-\lambda_2)}\left[\frac{2(\omega_1+\omega_2+\omega_4)-\lambda_2(1+\omega_4/\omega_3)}{\lambda_1/\omega+\omega/\lambda_1}+\frac{\lambda_1(1+\omega_4/\omega_3)-2(\omega_1+\omega_2+\omega_4)}{\lambda_2/\omega+\omega/\lambda_2}\right]. \quad (1)$$

Here N_i is the impurity concentration per unit volume, p is the degree of association, a is the lattice constant, and ω is the frequency of the applied field. ω_1, ω_2, ω_3, and ω_4 are the field-free jump frequencies of the cation vacancy, defined as follows: (i) ω_1, nn → nn; (ii) ω_2, nn → impurity; (iii) ω_3, nnn → nn; and (iv) ω_4, nn → nnn. The two relaxation times τ_1 and τ_2 are given by

$$(\tau_1)^{-1}=\lambda_1=\omega_1+\omega_2+2\omega_3+\omega_4+[(\omega_1+\omega_2-2\omega_3+\omega_4)^2+4\omega_3\omega_4]^{1/2},$$
$$(\tau_2)^{-1}=\lambda_2=\omega_1+\omega_2+2\omega_3+\omega_4-[(\omega_1+\omega_2-2\omega_3+\omega_4)^2+4\omega_3\omega_4]^{1/2}. \quad (2)$$